Quantitative transverse flow measurement using optical coherence tomography speckle decorrelation analysis

Xuan Liu,[1,*] Yong Huang,[1] Jessica C. Ramella-Roman,[2] Scott A. Mathews,[3] and Jin U. Kang[1]

[1]*Department of Electrical and Computer Engineering, The Johns Hopkins University, Baltimore, Maryland 21218, USA*

[2]*Department of Biomedical Engineering, The Catholic University of America, Washington, DC 20064, USA*

[3]*Department of Electrical Engineering and Computer Science, The Catholic University of America, Washington, DC 20064, USA*

**Corresponding author: xliu35@jhu.edu*

Received December 13, 2012; accepted January 18, 2013;
posted February 4, 2013 (Doc. ID 181684); published March 1, 2013

We propose an inter-Ascan speckle decorrelation based method that can quantitatively assess blood flow normal to the direction of the optical coherence tomography imaging beam. To validate this method, we performed a systematic study using both phantom and *in vivo* animal models. Results show that our speckle analysis method can accurately extract transverse flow speed with high spatial and temporal resolution. © 2013 Optical Society of America

OCIS codes: 110.4500, 030.6140.

Optical coherence tomography (OCT) has been shown to be able to measure subsurface microvasculature blood flow [1–7]. One widely used approach is optical Doppler tomography (ODT) that extracts Doppler frequency shift or broadening from the OCT signal to deduce blood flow with a component that is along the direction of the incident light beam [1–3]. ODT, however, is not sensitive to the flow in a plane normal to the incident beam. Alternatively, changes in OCT speckle pattern can be used to detect transverse flow without the longitudinal component. It has been shown that, by calculating interframe speckle variance (sv) of OCT images, svOCT is highly effective in detecting blood vessels [4,5] or even flow quantification [6]. However, Ren *et al.* demonstrated that svOCT was incapable of quantitatively measuring blood flow [7]. Although promising results were obtained from some recent studies on transverse flow measurement [8,9], it still remains challenging to quantify transverse flow using OCT. In this study, we propose to use cross-correlation coefficient (XCC) between Ascans for depth resolved quantitative transverse flow measurement.

A Cartesian coordinate system (x, y, z) is used to describe the 3D space in this Letter: z indicates the axial direction, x is the direction of the beam scanning, y is the direction normal to x-z plane. In this study, pure transverse flow in a direction normal to the beam scanning is considered; i.e., the flow is along the y axis. The 3D field reflectivity at an arbitrary time t is denoted as $r_s(x, y, z, t)$ and the corresponding OCT signal over the 3D space can be considered as the convolution of $r_s(x, y, z, t)$ with the OCT system's point spread function denoted as $h(x, y, z)$. Assuming an Ascan $I_1(z)$ is obtained at a spatial location (x_0, y_0) at time t_0 with infinitesimally short time, we can express $I_1(z)$ as Eq. (1) where $*$ indicates 3D convolution:

$$I_1(z) = [r_s(x, y, z, t_0) * h(x, y, z)]|_{x=x_0, y=y_0}. \quad (1)$$

Consider a subsequent Ascan $I_2(z)$ obtained at time $t_0 + \Delta t$. As the beam scans along axis x, the sampling point now becomes $(x_0 + \delta x, y_0)$ and $I_2(z)$ can be expressed as

$$I_2(z) = [r_s(x, y, z, t_0 + \Delta t) * h(x, y, z)]|_{x=x_0+\delta x, y=y_0}. \quad (2)$$

Due to the flow, the 3D field reflectivity of flowing blood at time $t_0 + \Delta t$ is a shifted version of the 3D field reflectivity at time t_0, as shown in Eq. (3):

$$r_s(x, y, z, t_0 + \Delta t) = r_s(x, y - \delta y, z, t_0). \quad (3)$$

In Eq. (3), y displacement δy equals $v\Delta t$ where v is the flow speed.

Writing the 3D convolution in Eq. (2) explicitly and plugging Eq. (3) into (2), we can rewrite Eq. (2) as

$$I_1(z) = [r_s(x, y, z, t_0) * h(x, y, z)]|_{x=x_0+\delta x, y=y_0-\delta y}. \quad (4)$$

Comparing Eq. (4) with Eq. (2), it is clear that taking an Ascan image at a point $(x_0 + \delta x, y_0)$ from the 3D object at time $t_0 + \Delta t$, is, in fact, equivalent to taking an Ascan image at a different imaging point $(x_0 + \delta x, y_0 - \delta y)$ from the 3D object at time t_0. Here, δx is the distance that the incident beam scans during time interval Δt and $\delta x = v_s \Delta t$ where v_s is the speed of beam scanning; δy is the distance scatters travel during the time interval Δt due to flow. As a result, if we consider a static object obtained by freezing $r_s(x, y, z, t)$ at time point t_0, and calculate the cross-correlation between an Ascan obtained at (x_0, y_0) and an Ascan obtained at $(x_0 + \delta x, y_0 - \delta y)$ from this frozen object, the result is the same as the cross-correlation between $I_1(z)$ and $I_2(z)$, which are Ascans obtained subsequently from the flowing object. In our previous work, we have developed a method to use XCC values to extract lateral displacement between Ascans from a static object [10]. The above-discussed equivalency implies that we can perform our speckle decorrelation analysis for quantitative flow measurement. The degree of correlation between adjacent,

over-sampled Ascans can be calculated by Pearson XCC, shown as Eq. (5) [10]:

$$\rho_{I_{x,y},I_{x+\delta x,y-\delta y}} = \frac{\langle [I_{x,y}(z) - \langle I_{x,y}(z)\rangle][I_{x+\delta x,y-\delta y}(z) - \langle I_{x+\delta x,y-\delta y}(z)\rangle]\rangle}{\sigma_{I_{x,y}(z)}\sigma_{I_{x+\delta x,y-\delta y}(z)}}. \tag{5}$$

In Eq. (5),$\langle\,\rangle$ indicates taking the mean value of the signal. Here $I_{x,y}(z)$ is the Ascan at (x, y) and $I_{x+\delta x,y-\delta y}(z)$ is the Ascan that is displaced by $(\delta x, -\delta y)$. $I_{x,y}(z)$ and $I_{x+\delta x,y-\delta y}(z)$, used in calculating Eq. (5), usually are the segments of Ascans containing a certain amount of pixels. $I_{Ix,y}(z)$ and $\sigma_{I_{x+\delta x,y-\delta y}(z)}$ are the square roots of variance for $I_{x,y}(z)$ and $I_{x+\delta x,y-\delta y}(z)$. The same segments in adjacent Ascans are used for the calculation of mean and variance.

As shown in our previous study, XCC between Ascans, denoted by ρ, depends on lateral displacement δl explicitly, as shown in Eq. (6) if the random field $r_s(x, y, z, t)$ flows Gaussian statistics:

$$\rho = \exp\left(-\frac{\delta l^2}{\delta w^2}\right). \tag{6}$$

In Eq. (6), w is the Gaussian beam waist and the lateral displacement is calculated as $\delta l = (\delta x^2 + \delta y^2)^{1/2} = (v_s^2 + v^2)^{1/2}\Delta t$. v_s can be calculated from the galvanometer scanner parameter and the focal length of the scanning lens, or obtained from a simple calibration experiment. Δt is determined by the line scan rate of the OCT system, therefore, we can obtain the flow speed v using XCC value, as shown in Eq. (7):

$$v = \pm\left[\sqrt{w^2\,\ln(1/\rho) - v_s^2}\right]//\Delta t. \tag{7}$$

The $\pm$ in Eq. (7) indicates that we are not able to determine the direction of the flow using a one-directional simple scanning pattern. We used the absolute value of v in this Letter to represent flow speed. It is worth mentioning that all the pixels, or a fraction of the pixels in adjacent Ascans, can be involved in the calculation of XCC using Eq. (5). When segments of Ascan at different imaging depths are used to obtain depth-resolved XCC, depth resolved transverse flow measurement can be obtained. Therefore, the speckle decorrelation analysis proposed in this Letter allows imaging transverse flow at different lateral and axial locations.

The spectral domain OCT system used in this study has been described in detail in our earlier papers [3,5]. Two phantoms were used in flow imaging experiments. In our phantom experiments, the speed of the flow was controlled using a precise syringe pump; the direction of beam scanning was performed normal to the flow. Finally, we performed the *in vivo* study using a mouse model.

To obtain the speckle pattern change due to the change in the flow rates, we imaged a home-made 300 μm microchannel pumped with bovine milk at a lateral step size of 0.6 μm. A Bscan image taken at zero flow rate is shown in Fig. 1(a). In Figs. 1(b)–1(e), we show the same area of the Bscan image indicated by the rectangular box

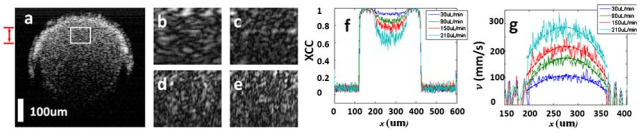

Fig. 1. (Color online) (a) OCT image of a circular microchannel filled with milk. (b)–(g) Bscan images at different flow rates of 30, 90, 150, and 210 μL/ min. (f) XCC as a function of lateral position, at different flow rates. (g) Calculated flow velocity across the flow channel fitted with parabolic.

in Fig. 1(a), at flow rates 30, 90, 150, and 210 μl/ min. The dimension of region of interest (ROI) in Figs. 1(b)–1(e) is 50 μm(axial) × 60 μm(lateral). Figures 1(b)–1(e) clearly show that the speckle size in the lateral direction becomes smaller at a larger flow rate, because as v_y becomes larger, the equivalent displacement δl, which is equal to $(v_s^2 + v^2)^{1/2}\Delta t$, also becomes larger. According to Eq. (6), this results in a smaller value of XCC or a speckle pattern in OCT image with a smaller grain size in the lateral dimension. Using a segment of the image over the depth range indicated by the red arrow in Fig. 1(a), we calculated XCC and show the results in Fig. 1(f), which corresponds to flow rates 30, 90, 150, and 210 μL/ min. It is clear that the overall XCC values are smaller for a larger flow rate, which is consistent with Eq. (6). In addition, we calculated v_y using Eq. (6) and show the results in Fig. 1(g). We also performed parabolic fitting using v_y values within the channel and show the results as thick, dashed curves in Fig. 1(g). The consistency between the experimental and the fitting curves indicates that the parabolic flow profiles can be extracted from speckle cross-correlation analysis. The nonzero flow signal at the capillary edge is due to speckle decorrelation induced by the structure of the sample, rather than speckle.

To further validate that the speckle decorrelation technique can be used to extract flow information quantitatively, we performed another set of phantom experiments using a microfluidic channel. The microfluidic device was built with a new, inexpensive methodology based on laser machining of common tape [11]. We used this structure because the planar structure of the flow channel does not create a lens effect for our scanning beam that would otherwise be introduced by a round flow channel; second, the incident beam diameter stays almost constant within the channel due to its small thickness. Also the optical signal attenuation can be neglected when light penetrates through the channel. The cross-section of the microchannel is illustrated in Fig. 2(a) and the corresponding OCT image is shown in Fig. 2(b). The OCT signal inside the flow channel was due to the

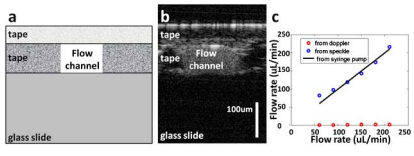

Fig. 2. (Color online) (a) Illustration of the cross-section of microfluidics. (b) OCT image of the cross-section of microfluidics. (c) Results of flow rate measurement from Doppler phase shift (red circles) and speckle decorrelation analysis (blue circles).

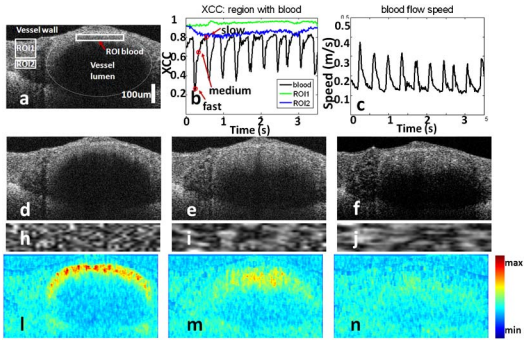

Fig. 3. (Color online) (a) Representative OCT image (Media 1). (b) Time sequences of XCC obtained from ROI corresponding to the area with blood flow, ROI1, and ROI2. (c) Blood flow speed calculated from XCC. (d)–(f) OCT images obtained at fast, medium, and slow blood flow speed. (h)–(j) central part of ROIs of Fig. 3. (d)–(f) chosen for XCC calculation. (l)–(n) 2D images of blood flow corresponding to Fig. 3. (d)–(f) Media 2 and Media 3.

scattering of bovine milk. OCT images were obtained at a 0.35 μm lateral step size. Flow rates obtained with speckle decorrelation analysis are shown as blue circles in Fig. 2(c). In Fig. 2(c), we also show the flow rate obtained from the reading of the syringe pump as the black curve. The consistency between the blue circles and the black curve shows that it is possible to measure transverse flow using speckle analysis, quantitatively. We also performed Doppler analysis on the same data set. As shown in Fig. 2 (red circles), the ODT signal cannot be used to extract transverse flow, because the Doppler phase shift is introduced by motion along the incident beam and has a much smaller range in flow rate measurement.

To show that our speckle analysis can be used to measure blood flow *in vivo*, we imaged a blood vessel from a live mouse and obtained 250 frames each with 2048(axial) × 1000(lateral) pixels. The animal study was conducted in accordance with the Johns Hopkins university animal care and use committee guidelines. The mouse was anesthetized and the femoral artery in the limb of the mouse was exposed for OCT imaging through a surgical procedure. With the CCD camera operated at its maximum speed (70 kHz line rate), the data acquisition took 3.6 s, which contained multiple cardiac cycles (Media 1). One of the Bscan images of the blood vessel is shown in Fig. 3(a). To show the temporal variation of blood flow, we selected rectangular ROIs corresponding to blood, as illustrated by the red–dashed rectangle in Fig. 3(a). Afterward, we calculated XCC values at different lateral locations within the ROI, averaged the values of XCC obtained from the ROI of each Bscan, and showed the result as the black curve in Fig. 3(b). For comparison, we also used nonblood regions indicated by ROI1 and ROI2 in Fig. 3(a) to calculate the averaged XCC. The results are shown as green (ROI1) and blue (ROI2) curves in Fig. 3(b). In Fig. 3(b), the black curve shows periodical pulsation that does not exist in the green and blue curves, indicating the pulsation is due to blood flow speed variation in cardiac cycles rather than bulk tissue motion in respiration cycles. Blood-flow speed within blood ROI was calculated with XCC values and shown as a black curve in Fig. 3(c). We performed Fourier analysis on the obtained blood flow graph and obtained a frequency peak at 2.8 Hz corresponding to a heart beat rate of 168 beats per minute. To demonstrate the difference in speckle pattern at different flow speeds, in Figs. 3(d)–3(f), we show OCT images corresponding to fast, medium, and slow flow as indicated by red circles in Fig. 3(b). The variation of speckle size can be seen more clearly in Figs. 3(h)–3(j), which are the central part of ROIs of Figs. 3(d)–3(f) chosen for XCC calculation. To further obtain transverse blood flow image $v(x,z)$, we took two adjacent Ascans at lateral coordinate x; calculated ρ using Eq. (5) using 16-pixel segments (corresponding to an axial resolution of 20 μm) centered at axial coordinate z, and calculated flow speeds using Eq. (6). With laterally and axially resolved XCC values and flow speeds, we obtained flow images as shown in Media 2. In Figs. 3(l)–3(n), we show flow images obtained from OCT images in Figs. 3(d)–3(f) using speckle decorrelation analysis. Figures 3(l)–3(n) show a large, medium, and small flow signal, which is consistent with Fig. 3(d). We overlayed the 250 frames of OCT structural image and tabulated flow image using HSV colormap in Media 3 that highlights blood and shows blood flow variation (H; hue takes the value of 0, S; saturation takes the value from flow image, V; value takes the value from OCT structural image).

The sensitivity of our transverse flow measurement depends on scanning pattern, system signal-to-noise ratio, speckle statistics and sample properties, such as absorption and scattering coefficients [12].

We thank Mr. Qi Mao for his help in the mouse experiments. The research reported in this Letter was supported in part by NIH BRP grants 1R01 EB 007969, NIH/NIE R011R01EY021540-01A1.

References

1. Z. P. Chen, T. E. Milner, S. Srinivas, X. Wang, A. Malekafzali, M. J. C. van Gemert, and J. S. Nelson, Opt. Lett. **22**, 1119 (1997).
2. R. K. Wang, S. L. Jacques, Z. Ma, S. Hurst, S. R. Hanson, and A. Gruber, Opt. Express **15**, 4083 (2007).
3. Y. Huang, X. Liu, and J. U. Kang, Biomed. Opt. Express **3**, 2162 (2012).
4. A. Mariampillai, B. A. Standish, E. H. Moriyama, M. Khurana, N. R. Munce, M. K. K. Leung, J. Jiang, A. Cable, B. C. Wilson, I. A. Vitkin, and V. X. D. Yang, Opt. Lett. **33**, 1530 (2008).
5. X. Liu, K. Zhang, Y. Huang, and J. U. Kang, Biomed. Opt. Express **2**, 2995 (2011).
6. A. Mariampillai, M. K. Leung, M. Jarvi, B. A. Standish, K. Lee, B. C. Wilson, I. A. Vitkin, and V. X. D. Yang, Opt. Lett. **33**, 1530 (2010).
7. H. Ren, C. Du, and Y. Pan, Opt. Lett. **37**, 1388 (2012).
8. J. Barton and S. Stromski, Opt. Express **13**, 5234 (2005).
9. Z. Y. Shen, M. Wang, Y. H. Ji, Y. H. He, X. S. Dai, P. Li, and H. Ma, Laser Phys. Lett. **8**, 318 (2011).
10. X. Liu, Y. Huang, and J. U. Kang, Opt. Express **20**, 16567 (2012).
11. L. Luu, P. A. Roman, S. A. Mathews, and J. C. Ramella-Roman, Biomed. Opt. Express **3**, 1350 (2012).
12. X. Liu, J. C. Ramella-Roman, Y. Huang, Y. Guo, and J. U. Kang, J. Opt. Soc. Am. A **30**, 51 (2013).